Journal of Sound and Vibration (2002) **252**(4), 739–749
doi:10.1006/jsvi.2001.3802, available online at http://www.idealibrary.com on IDEAL®

DYNAMIC RESPONSE OF A CONSTRAINED AXIALLY LOADED BEAM

I. SVENSSON

Division of Solid Mechanics, Lund University, Box 118, *S*-221 00 *Lund, Sweden.*
E-mail: ingrid@solid.lth.se

(*Received* 11 *September* 2000, *and in final form* 8 *June* 2001)

A dynamic beam system loaded harmonically in the axial direction and constrained in the transverse direction is modelled using different theoretical descriptions. Results from an experimental set-up are compared to calculations using Bernoulli as well as Timoshenko beam theories. Some results from investigations of this beam system unveiling its chaotic nature have earlier been presented, but here the refining of Timoshenko theory is done in order to get a better understanding of the influence of the impacts on the beam motion. The free motion of the beam is described as a finite sum of modes, while at impact an infinite number of modes is considered, albeit approximately. These ideas were also used for the Bernoulli beam, but modifications will be made here to account for the modal equations of fourth order in time for the Timoshenko beam. The investigation is complemented with new experiments.

1. INTRODUCTION

Systems undergoing deterministic loading and exhibiting chaotic behaviour have been extensively studied in the literature. One example is the study made by Li *et al.* [1], where chaotic regions in the parameter space for a constrained pipe conveying fluid were detected. Mechanical oscillators with play or amplitude constraining stops are other examples of systems with chaotic behaviour for special choices of loading parameters. Here, a study made by Moon and Shaw [2] of a harmonically loaded non-linear beam system can be mentioned. The clamped end of a cantilever beam was excited with different choices of the driving frequency and load amplitude, and the non-linearity is this system arose from the boundary condition at the free end of the cantilever beam. The tip of the beam was free to move in one direction but encountered a stop, which pinned the tip displacement exceeded a critical value in the other direction. Chaotic vibrations were observed both in experiments and simulations for certain values of the loading parameters.

The object of the present study is an axially loaded beam with a one-sided constrained lateral deflection. The load varies sinusoidally with time and the ends of the beam are pinned such that only symmetric motions are considered. For special values of the amplitude and frequency of the applied load, chaotic oscillations have been detected, both experimentally and in simulations [3].

Earlier comparisons between experimental results and computer simulations of the beam motion showed good qualitative correspondence [4]. The quantitative correspondence, however, was not quite good, particularly as regards the duration of time spent in contact with the constraint. The simulated contact times were always shorter, regardless of the model used to describe the impacts.

0022-460X/02/$35.00

In this work, the effect of refining the beam model from Bernoulli to Timoshenko theory is investigated. Timoshenko beam theory has been used earlier in stability analysis (e.g. references [5, 6]. In those studies, the reason for using the refined theory was mainly not to restrict the results to long slender beams. When using Timoshenko theory, transverse shear deformations are also accounted for and thereby the results are also valid for thick beams. The reason for using Timoshenko theory in this study is quite different. Following Fung [7], the phase velocities for the higher order deflection modes are lower when the theory is refined. This will cause high order modes to propagate slower for the Timoshenko beam than for the Bernoulli beam, and the extended contact times may then be expected.

More experiments have been performed using the set-up described in reference [4], and a more systematic analysis of the results has been performed in such a way that direct comparisons with simulations are obtained.

2 FORMULATION OF THE PROBLEM

2.1. TIMOSHENKO THEORY

A Kelvin material is chosen and if for uniaxial stress conditions, i.e., $\sigma = \sigma_{11}$, it is assumed that $\varepsilon_{33} = -\nu\varepsilon_{11}$, where ν is the Poisson's ratio, then it follows from reference [8] that the constitutive relation between the stress σ and strain ε becomes

$$\sigma = E\varepsilon + \eta\dot{\varepsilon}, \tag{1}$$

where E is Young's modulus and η is a viscosity parameter. In shearing, one has

$$\tau = G\gamma + \frac{G}{E}\eta\dot{\gamma}, \tag{2}$$

where τ is the shear stress, γ is the shear strain and G is the shear modulus. Following the Timoshenko beam theory, the deformation of the beam in Figure 1 with length L, bending stiffness EI, shear stiffness GA and mass density ρ is described by the longitudinal displacement u along the neutral axis, the transverse displacement w and the rotation of the cross-section ψ. Note that the co-ordinates x and y are referred to the undeformed co-ordinate system. According to Figure 1, the transverse constraint is located at the

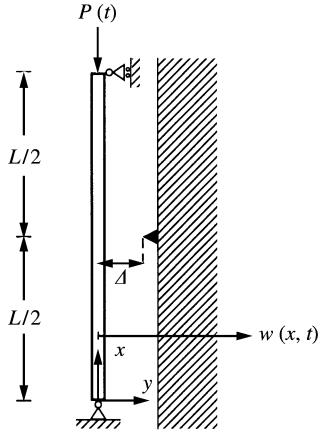

Figure 1. The system under study.

midpoint of the beam. The rotation is related to the bending moment M through

$$M = -EI\frac{\partial\psi}{\partial x} - \eta I\frac{\partial^2\psi}{\partial x\partial t}. \tag{3}$$

The rotation and the transverse displacement are coupled to the transverse shear force T via

$$T = k'GA\left(\frac{\partial w}{\partial x} - \psi\right) + k'\eta A\frac{G}{E}\left(\frac{\partial^2 w}{\partial x\partial t} - \frac{\partial\psi}{\partial t}\right). \tag{4}$$

The factor k' is the ratio of the average shear strain over the cross-section to the maximum shear strain at the centroid. The value of this factor is chosen differently by different authors in the literature. For elasticity and a rectangular cross-section, Fung [7] using elementary beam theory suggests that $k' = 2/3$, whereas Timoshenko *et al.* [9] give the value $k' = 5/6$. This factor is discussed in detail by Cowper [10] and we shall adopt here the value $k' = 5/6$.

Finally, the longitudinal displacement is related to the normal force N through

$$N = EA\frac{\partial u}{\partial x} + \eta A\frac{\partial^2 u}{\partial x\partial t}. \tag{5}$$

The equations of motion can be derived from Figure 2. In the transverse direction,

$$\rho A\frac{\partial^2 w}{\partial t^2} = q + \frac{\partial T}{\partial x}, \tag{6}$$

where q is the loading per unit length. Likewise, the longitudinal direction yields

$$\rho A\frac{\partial^2 u}{\partial t^2} = \frac{\partial N}{\partial x}, \tag{7}$$

whereas for the rotation it follows that

$$\rho I\frac{\partial^2\psi}{\partial t^2} = -\frac{\partial M}{\partial x} + T - N\frac{\partial w}{\partial x}. \tag{8}$$

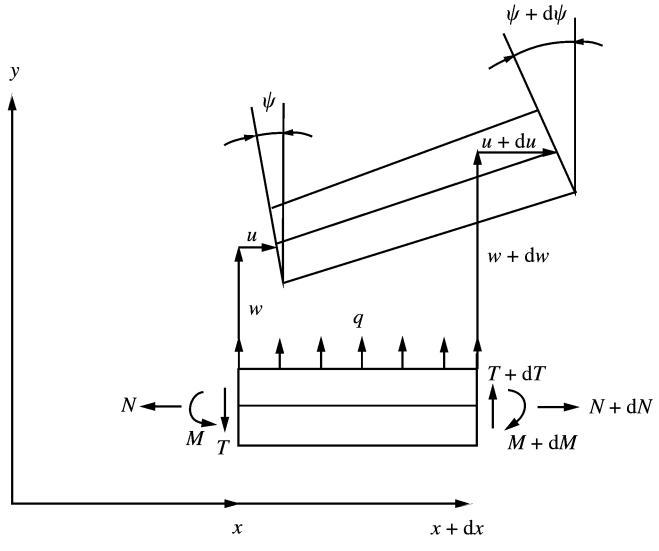

Figure 2. Loading of beam with length dx and corresponding deformations. The directions of the normal force N, the shear force T and the bending moment M all refer to an undeformed co-ordinate system.

The axial force P, as shown in Figure 1, is measured positive when it is compressive and is assumed to oscillate harmonically with time, $P = P_0 \cos vt$. In this study, the period of oscillation, $2\pi/v$, is at least one order of magnitude higher than the time of longitudinal waves to travel the length of the beam, $L/\sqrt{E/\rho}$, and then, if the damping in equation (5) is neglected, then the axial force can be assumed to be independent of the co-ordinate x running along the beam axis, i.e., $N(x, t) = -P_0 \cos vt$. The longitudinal motion is then given by the steady state solution

$$u(x, t) = -x \frac{P_0}{EA} \cos vt, \tag{9}$$

where the boundary condition $u = 0$ at $x = 0$ is taken into account.

It will be assumed to be a homogeneous material and that the cross-section is constant along the beam. Moreover, to simplify the analysis, we shall ignore the viscous term in the expression for the shear force T in equation (4), which certainly is of only minor influence. From equations (4) and (6), it is then possible to find an expression for $\partial\psi/\partial x$. With expressions (3) and (4) inserted into equation (8) and then differentiation with respect to x it is possible to eliminate the rotation and obtain the following equation, which is fifth order in time and space for the transverse motion:

$$\frac{1}{c_0^2 c_Q^2} \frac{\partial^4 w}{\partial t^4} - \frac{\eta}{E c_Q^2} \frac{\partial^5 w}{\partial x^2 \partial t^3} - \left(\frac{1}{c_0^2} + \frac{1}{c_Q^2}\right) \frac{\partial^4 w}{\partial x^2 \partial t^2} + \frac{1}{c_0^2 R^2} \frac{\partial^2 w}{\partial t^2} + \frac{\eta}{E} \frac{\partial^5 w}{\partial x^4 \partial t} + \frac{\partial^4 w}{\partial x^4} + \frac{P_0}{EI} \frac{\partial^2 w}{\partial x^2} \cos vt$$

$$= \frac{1}{c_0^2 c_Q^2} \frac{1}{\rho A} \frac{\partial^2 q}{\partial t^2} + \frac{1}{c_0^2 R^2} \frac{q}{\rho A} - \frac{1}{c_Q^2} \frac{1}{\rho A} \frac{\partial^2 q}{\partial x^2} - \frac{\eta}{E c_Q^2 \rho A} \frac{\partial^3 q}{\partial x^2 \partial t}, \tag{10}$$

where the parameters c_0, c_Q and R are defined as

$$c_0 = \sqrt{\frac{E}{\rho}}, \qquad c_Q = \sqrt{\frac{k'G}{\rho}}, \qquad R = \sqrt{\frac{I}{A}}. \tag{11}$$

Bearing the boundary conditions at the ends of the beam in mind, it is obvious that the deflection can be written in the form of a Fourier sine series with $f_i(t)$ denoting the Fourier coefficients:

$$w(x,\ t) = \sum_{i=1}^{\infty} f_i(t)\ \sin \frac{i\pi x}{L}. \tag{12}$$

Inserting into equation (10), multiplying by $\sin(j\pi x/L)$, where $j = 1, 2, \ldots$ and integrating over the length of the beam gives

$$\frac{1}{c_0^2 c_Q^2} \frac{\mathrm{d}^4 f_j}{\mathrm{d}t^4} + \frac{\eta}{E c_Q^2} \frac{j^2\pi^2}{L^2} \frac{\mathrm{d}^3 f_j}{\mathrm{d}t^3} + \left[\frac{j^2\pi^2}{L^2}\left(\frac{1}{c_0^2} + \frac{1}{c_Q^2}\right) + \frac{1}{c_0^2 R^2}\right] \frac{\mathrm{d}^2 f_j}{\mathrm{d}t^2} + \frac{\eta}{E} \frac{j^4\pi^4}{L^4} \frac{\mathrm{d}f_j}{\mathrm{d}t}$$

$$+ \frac{j^2\pi^2}{L^2}\left(\frac{j^2\pi^2}{L^2} - \frac{P_0}{EI} \cos vt\right) f_j = \frac{2}{\rho A L}\left[\frac{1}{c_0^2 c_Q^2} \int_0^L \frac{\partial^2 q}{\partial t^2} \sin \frac{j\pi x}{L} \mathrm{d}x\right.$$

$$+ \frac{\eta}{E} \frac{1}{c_Q^2} \frac{j^2\pi^2}{L^2} \int_0^L \frac{\partial q}{\partial t} \sin \frac{j\pi x}{L} \mathrm{d}x + \left(\frac{1}{c_0^2 R^2} + \frac{1}{c_Q^2} \frac{j^2\pi^2}{L^2}\right) \int_0^L q \sin \frac{j\pi x}{L} \mathrm{d}x$$

$$\left. - \frac{j\pi}{L}((-1)^j - 1)\left(\frac{\eta}{c_Q^2 E} \frac{\partial q_0}{\partial t} + \frac{1}{c_Q^2} q_0\right)\right]. \tag{13}$$

Thus, the equations determining the Fourier coefficients, one for each mode shape, are decoupled and can be solved separately. Notice that the terms originally containing second order derivatives of the transverse load with respect to the co-ordinate along the beam, $\partial^2 q/\partial x^2$ and $\partial^3 q/\partial x^2 \partial t$, have been partially integrated twice under the assumption of q being a symmetric function over the length of the beam L, i.e., $q(x=0) = q(x=L) = q_0$ and $\partial q/\partial t(x=0) = \partial q/\partial t\,(x=L) = \partial q_0/\partial t$.

2.2. BERNOULLI THEORY

When using Bernoulli beam theory and ignoring the rotational inertia effect, but otherwise assuming the same material behaviour as before, equation (1), the resulting partial differential equation becomes

$$EI\frac{\partial^4 w}{\partial x^4} + P_0\frac{\partial^2 w}{\partial x^2}\cos \nu t + \eta I\frac{\partial^5 w}{\partial x^4 \partial t} + \rho A\frac{\partial^2 w}{\partial t^2} = q. \tag{14}$$

Following the same procedure as for the Timoshenko beam, the result after Fourier expansion, multiplication by $\sin j\pi x/L$ and integration over the length of the beam gives

$$\rho A\frac{\mathrm{d}^2 f_j}{\mathrm{d}t^2} + \eta I\frac{j^4\pi^4}{L^4}\frac{\mathrm{d}f_j}{\mathrm{d}t} + \left(EI\frac{j^4\pi^4}{L^4} - \frac{j^2\pi^2}{L^2}P_0\cos \nu t\right)f_j = \frac{2}{L}\int_0^L q\sin\frac{j\pi x}{L}\mathrm{d}x. \tag{15}$$

Equation (15) denotes the Fourier coefficients for the Bernoulli beam and corresponds to equation (13) for the Timoshenko beam.

2.3. MODELLING THE IMPACTS

The influence of the impacts on the transverse deflection is contained in the external transverse load, $q(x, t)$. For simplicity and according to Figure 1, the impact is considered as a point load situated at the midpoint of the beam, $x = L/2$, and a distance, Δ, from the rest position of the beam, i.e.,

$$q(x,t) = \begin{cases} \delta(x - \frac{L}{2})Q(t) & \text{if } w(L/2,t) = \Delta, \\ 0 & \text{if } w(L/2,t) < \Delta. \end{cases} \tag{16}$$

Here, $\delta(x)$ is the Dirac delta function, and Q denotes the force acting at the midpoint of the beam. During impact, equation (13) becomes

$$\begin{aligned} &\frac{\mathrm{d}^4 f_j}{\mathrm{d}t^4} + \frac{\eta}{E}c_0^2\frac{j^2\pi^2}{L^2}\frac{\mathrm{d}^3 f_j}{\mathrm{d}t^3} + \left[\frac{j^2\pi^2}{L^2}(c_Q^2 + c_0^2) + \frac{c_Q^2}{R}\right]\frac{\mathrm{d}^2 f_j}{\mathrm{d}t^2} \\ &\quad + \frac{\eta}{E}c_0^2 c_Q^2\frac{j^4\pi^4}{L^4}\frac{\mathrm{d}f_j}{\mathrm{d}t} + c_0^2 c_Q^2\frac{j^2\pi^2}{L^2}\left(\frac{j^2\pi^2}{L^2} - \frac{P_0}{EI}\cos \nu t\right)f_j \\ &= (-1)^{(j-1)/2}\frac{2}{\rho A L}\left[\frac{\mathrm{d}^2 Q}{\mathrm{d}t^2} + c_0^2\frac{\eta}{E}\frac{j^2\pi^2}{L^2}\frac{\mathrm{d}Q}{\mathrm{d}t} + \left(\frac{c_Q^2}{R^2} + c_0^2\frac{j^2\pi^2}{L^2}\right)Q\right], \quad j \text{ odd}. \end{aligned} \tag{17}$$

Here, the derivations of the influence of the impacts are presented only for the Timoshenko beam, but the procedure for the Bernoulli beam is analogous starting from equation (15) instead of equation (13), this can be followed in reference [3].

No antisymmetric mode ($j = 2, 4, \ldots$) can be invoked by the impacts because the right-hand side of equation (18) is zero for the antisymmetric modes, i.e., the modes with even mode numbers. It then follows that there will never be any antisymmetric mode present in motion if the initial condition contains only symmetric modes. In the following, only symmetrical modes will be considered, i.e., j is odd.

Since the wall is considered to be infinitely stiff, the deflection condition at impact is that the total deflection equals the distance between the undeflected beam midpoint and the point constraint, i.e.,

$$f_1 - f_3 + f_5 - \cdots = \sum_{j=1}^{\infty} (-1)^{(j-1)/2} f_j = \Delta, \quad j \text{ odd}. \tag{18}$$

In practice, there is always an upper bound of how many modes can be taken into account in the numerical calculations. Let us consider n to be the highest mode number taken into account for the free motion. At impact it is possible to introduce some simplifications for the mode equations with mode numbers $j > n$. If n is large enough, then the first simplification of equation (18) is to ignore the $\cos vt$ term since $j^2\pi^2/L^2$ becomes much greater than the term P_0/EI for $j > n$ and n sufficiently large. This simplification can also be motivated by comparing the load amplitude P_0, which in both the simulations and the experiments is in the range of the first buckling load. $P_{c,1}$, with the buckling load for the mode j, $P_{c,j}$. From reference [11]

$$P_{c,j} = j^2 P_{c,1}, \tag{19}$$

which ensures that the load amplitude in the experiments and simulations is much lower than the critical load for the modes with mode numbers $j > n$.

The next simplification is based on the fact that the contact time is much larger than the period of the mode number n. Due to damping, the transients from the homogeneous solution of equation (18) are then damped out and the fourth, third, second and first order time derivatives on the left-hand side of equation (18) can then be neglected for $j > n$. One can therefore conclude that for $j > n$ and n sufficiently large, equation (18) will only have the particular solution

$$f_j = (-1)^{(j-1)/2} \frac{1}{c_0^2 c_Q^2} \frac{2L^3}{\rho A \pi^4} \left[\frac{1}{j^4} \frac{\mathrm{d}^2 Q}{\mathrm{d}t^2} + c_0^2 \frac{\eta}{E} \frac{\pi^2}{L^2} \frac{1}{j^2} \frac{\mathrm{d}Q}{\mathrm{d}t} + \left(\frac{1}{j^4} \frac{c_Q^2}{R^2} + \frac{1}{j^2} \frac{c_0^2 \pi^2}{L^2} \right) Q \right], \quad j \text{ odd} \quad \text{and} \quad j > n. \tag{20}$$

The infinite sum in the deflection condition in equation (18) can then be divided into two parts, i.e.,

$$\sum_{j=1}^{n} (-1)^{(j-1)/2} f_j + \sum_{j=n+2}^{\infty} (-1)^{(j-1)/2} f_j = \Delta, \tag{21}$$

where the second sum can now be expressed in terms of the particular solutions of equation (20) for the modes with mode number $j > n$, i.e.,

$$\sum_{j=n+2}^{n} (-1)^{(j-1)/2} f_j = \frac{1}{c_0^2 c_Q^2} \frac{2L^3}{\rho A \pi^4} \left\{ \frac{\mathrm{d}^2 Q}{\mathrm{d}t^2} \left[\sum_{j=1}^{\infty} \frac{1}{j^4} - \sum_{j=1}^{n} \frac{1}{j^4} \right] + \frac{\mathrm{d}Q}{\mathrm{d}t} c_0^2 \frac{\eta}{E} \frac{\pi^2}{L^2} \left(\sum_{j=1}^{\infty} \frac{1}{j^2} - \sum_{j=1}^{n} \frac{1}{j^2} \right) + Q \left[\frac{c_Q^2}{R^2} \left(\sum_{j=1}^{\infty} \frac{1}{j^4} - \sum_{j=1}^{n} \frac{1}{j^4} \right) + \frac{c_0^2 \pi^2}{L^2} \left(\sum_{j=1}^{\infty} \frac{1}{j^2} - \sum_{j=1}^{n} \frac{1}{j^2} \right) \right] \right\}. \tag{22}$$

The infinite sums in equation (22) are determined through

$$\sum_{j=1}^{\infty}\frac{1}{j^2}=\sum_{k=1}^{\infty}\frac{1}{(2k-1)^2}=\frac{\pi^2}{8},\quad \sum_{j=1}^{\infty}\frac{1}{j^4}=\sum_{k=1}^{\infty}\frac{1}{(2k-1)^4}=\frac{\pi^4}{96},$$

where j is odd but k denotes all integers. The deflection condition at contact in equation (21) can now be written as

$$C_1\frac{\mathrm{d}^2Q}{\mathrm{d}t^2}+C_2\frac{\mathrm{d}Q}{\mathrm{d}t}+C_3Q=C_4\left(\Delta-\sum_{j=1}^{n}(-1)^{(j-1)/2}f_j\right) \tag{23}$$

with the constants C_1, C_2, C_3 and C_4 given by

$$C_1=\frac{\pi^4}{96}-\sum_{j=1}^{n}\frac{1}{j^4},\qquad C_2=c_0^2\frac{\eta}{E}\frac{\pi^2}{L^2}\left(\frac{\pi^2}{8}-\sum_{j=1}^{n}\frac{1}{j^2}\right),$$

$$C_3=\frac{c_Q^2}{R^2}\left(\frac{\pi^4}{96}-\sum_{j=1}^{n}\frac{1}{j^4}\right)+\frac{c_0^2\pi^2}{L^2}\left(\frac{\pi^2}{8}-\sum_{j=1}^{n}\frac{1}{j^2}\right),\qquad C_4=\frac{\rho A\pi^4}{2L^3}c_0^2c_Q^2. \tag{24}$$

The computation is therefore as follows. The free motion of the beam is calculated from equation (18) with mode numbers up to and including n and the right sides of these equations being equal to zero. An impact is then detected with the impact deflection condition of equation (18), where only the first n modes are considered. Then, the differential equation for Q, equation (23), is solved with the actual values of $f_1, f_3, \ldots, f_n$ determining the right side. The solutions for Q, $\mathrm{d}Q/\mathrm{d}t$ and $\mathrm{d}^2Q/\mathrm{d}t^2$ are now put into the modal equations for type equation (18) and in the next time step the modal equations are solved with their right sides differing from zero.

3. RESULTS

Results from numerical simulations as well as experiments will be presented and compared here. The experimental set-up can be described as a horizontally oriented steel beam with hinges at both ends. One of the hinges is connected to an electro-magnetic vibrator and the other to a load cell. The constraint is situated at the beam midpoint, a small distance from the undeflected beam. The deflection and the velocity of the beam midpoint are measured by a laser displacement meter. A more detailed description of the set-up is presented in reference [4]. The simulations are performed with the Matlab Ode Suite [12] using Runge–Kutta methods of second order.

In Figure 3(a), a measured phase plot is presented. This phase plot can be compared with the phase plots derived from numerical implementations of the Timoshenko beam theory, Figure 3(b). In both simulations, the midpoint deflection and the midpoint velocity are followed from the same initial values and over the same time span. The loading parameters are $P_0 = 0{\cdot}73\ P_1^c$ and $v = 2{\cdot}0\ \omega_1$, where P_1^c is the first buckling load and ω_1 is the first eigenfrequency of the unconstrained beam.

The similarities of the experimental and simulated phase plots are evident. Further, it can be concluded from Figure 3(b) that the influence from the higher order modes is damped out during the free motion and it is sufficient to use four modes in the simulations.

Results from calculations with the two beam hypotheses are presented in Figure 4. The midpoint deflection and the midpoint velocity are followed from the same initial values and over the same time interval for the two simulations. There is no essential difference between

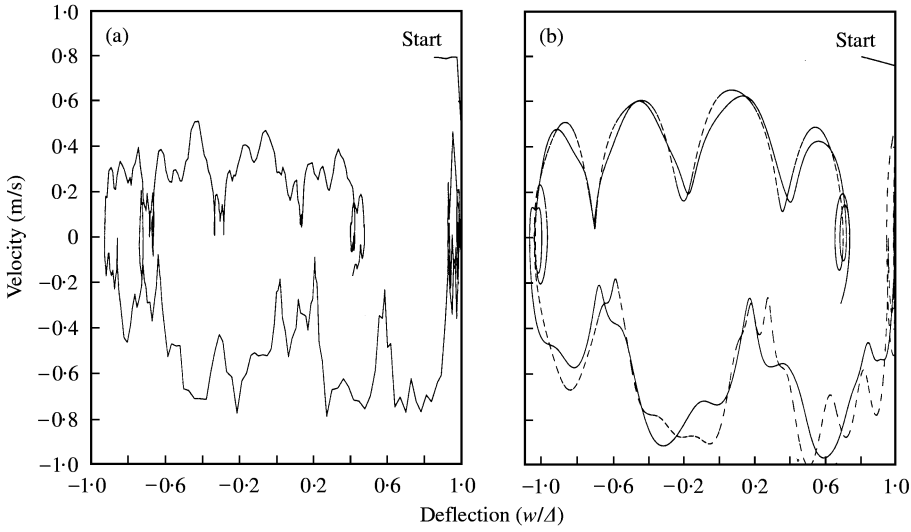

Figure 3. Phase plots obtained from (a) experimental data and (b) Timoshenko data. The calculations are performed with four modes for the free motion for the solid trajectory and with 10 modes for the dashed trajectory. The damping coefficient is $\eta = 0{\cdot}00002s * E$.

the two curves. Evidently, as can be seen in the following, cf., Figure 6, the two beam models will give the same contact times so the earlier discussed problem with the simulated contact times being too short compared to the experimental ones will remain thus when using Timoshenko beam theory, and therefore other explanations of this phenomenon must be sought. This is certainly surprising since the phase velocities for the higher order modes according to reference [7] are lower for the Timoshenko beam theory than for Bernoulli beam theory. For the Timoshenko beam theory these higher order modes will, therefore, propagate slowly compared to Bernoulli theory and extended contact times may then be expected. Figure 4 and, further on, Figure 6 clearly illustrate that this effect is not dominant for the problem in question and the only remaining phenomena that is open for a more accurate modelling is the impact event itself.

Moreover, the computation time for the Timoshenko beam turned out to be much longer than for the Bernoulli beam. This is not surprising since the differential equations are of fourth order for the Timoshenko beam, so the implementation includes twice as many state variables. Furthermore, during contact, one additional differential equation of second order for the contact force has to be solved for the Timoshenko beam.

In Figure 5, parts of the simulations presented in Figure 4 are shown in a deflection versus time diagram. The phenomenon of multiple impacts is evident in Figure 5. A complete impact, i.e., the process after which the beam eventually has changed its direction of motion, consists of a series of bounces occurring very closely in time. This behaviour was also observed in the experiments. To have a quantity by which experiments and simulations can be compared, it turned out to be more meaningful to look at the whole impact process and not the separate bounces. In the following comparisons, the dwell time is then defined as the time when the midpoint deflection exceeds 0·95, cf., Figure 5. To be consistent, the value $0{\cdot}95\Delta$ is also chosen in the experiments to define dwell time.

With this definition of the duration of an impact, a systematic investigation of the dwell times for the two beam models has been performed. The initial deflection of the first mode was put equal to $0{\cdot}95\Delta$, and the initial velocity of the first mode was varied from 0·01 m/s up to 1 m/s. All other state variables are initially set to zero.

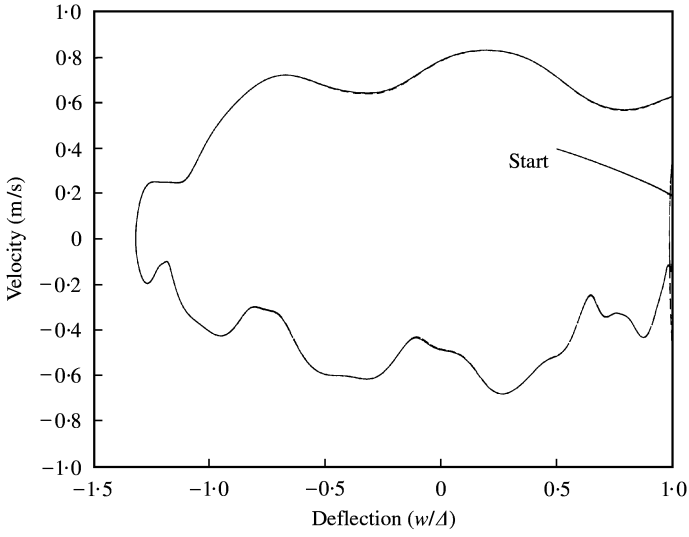

Figure 4. The trajectory predicted by Timoshenko (———) and Bernoulli beam theory, (– – – –). In both cases, four modes are used for the free motion, damping coefficient $\eta = 0{\cdot}00002s * E$ and loading parameters $P_0 = 0{\cdot}5P_1^c$ and $v = 2{\cdot}0\omega_1$.

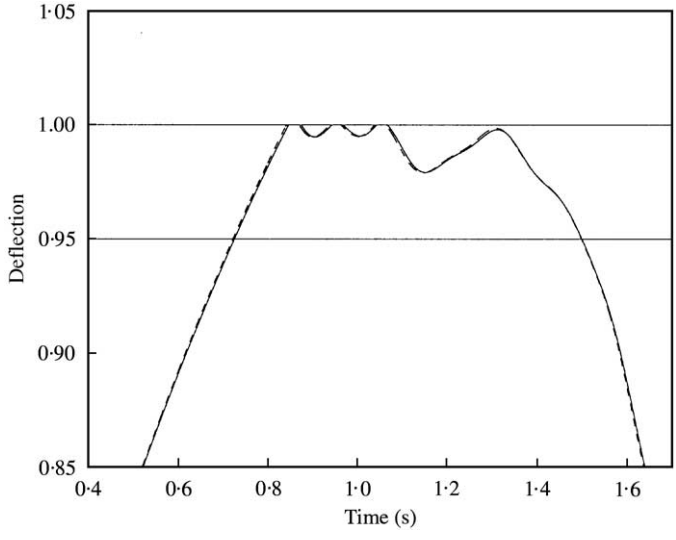

Figure 5. Time versus deflection for the beam midpoint. The deflection border of $0{\cdot}95\Delta$ for measuring the dwell time is also drawn in the diagram.

The first observation made in Figure 6 in agreement with the two beam models. The jump that occurs when the initial velocity, which is equivalent to the impact velocity, is about 0·6 m/s, where the dwell time is nearly halved, is apparent. As will be shown later on, this jump can be explained as the limit between two different types of impact. If the velocity of impact is higher than 0·6 m/s, then the dwell time turns out to be relatively small but the impact is always immediately followed by another impact with a low velocity and about the same dwell time as the first.

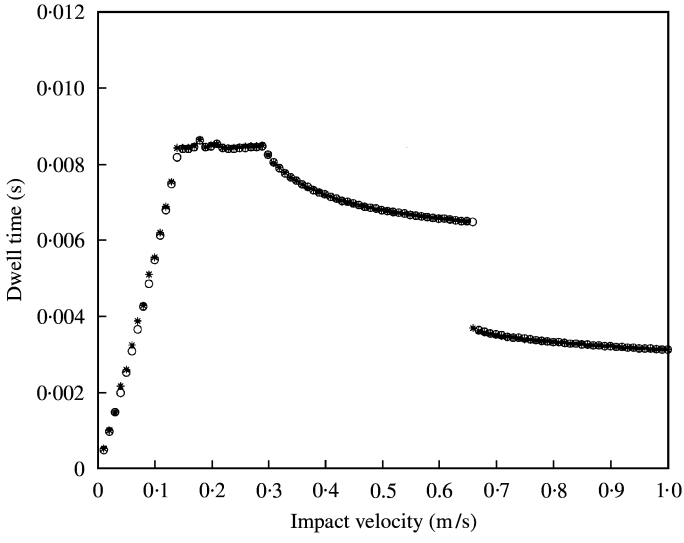

Figure 6. Systematic control of dwell times. The results from the simulation of the Bernoulli beam are marked with (∗), and the results of the Timoshenko beam simulation are marked with (○). The loading parameters are $P_0 = 0{\cdot}5\,P_1^c$ and $v = 2{\cdot}0\omega_1$ and the damping coefficient is $\eta = 0{\cdot}00002s * E$ in both simulations.

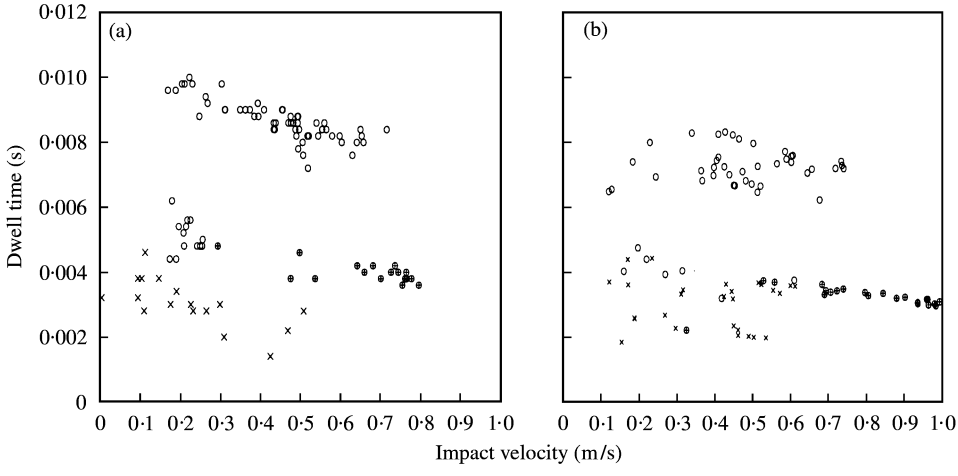

Figure 7. Dwell times obtained from (a) experimental data and (b) Bernoulli data. Loading parameters are $P_0 = 0{\cdot}7P_1^c$ and $v = 2{\cdot}0\omega_1$ and the damping coefficient in the simulation is $\eta = 0{\cdot}00002 * E$. A single impact is marked with (○), the first impact of a double impact is marked with (⊕) and the second one with (×).

In Figure 7(a), a series of impacts recorded experimentally is presented. During these experiments it was observed that the impacts with short dwell times, 4–5 ms, occur very closely in time, i.e., the beam bounced twice before leaving the constraint. It then seems natural to introduce the definition of a double impact: if the beam did not pass the undeflected position between two impacts, then the two impacts were defined as one double impact. In Figure 7(a), a single impact is marked with (○), the first bounce of a double impact is marked with (⊕) and the second one with (×). It can also be noted that the sum of the dwell times for a complete double impact is about the same as for a single impact, 8–9 ms. There were no triple or higher order impacts recorded.

A series of impacts was recorded during a simulation of the Bernoulli beam (Figure 7(b)) with equivalent markings for comparison with the experimental data in Figure 7(a). No impacts of order higher than two were observed in this simulation. A complete impact, single or the sum of a double, is measured to about 8 ms and this is in good agreement with the experiments. Also, the minimum level of approximately 0·5–0·6 m/s for which double impacts occur is observed both experimentally and in simulations.

It can be noted here that if the deflection limit for defining impact, instead was chosen as, e.g., $w = 0{\cdot}98\Delta$, triple or even impact processes consisting of four bounces is observed both in the simulations and in the experiment. Then, the corresponding diagrams to Figure 7 would show one level of dwell time equal to one-third of the dwell time of a complete impact process and even a level at one-fourth in the presence of four bounces.

4. CONCLUSIONS

One of the reasons for using a Timoshenko beam theory was the expectation of improving the agreement between simulated and observed dwell times. However, it turned out that the effect of the lower-phase velocities of the higher order modes of the Timoshenko beam in the present case is quite small that it is hardly worth the extra computation time to introduce the Timoshenko beam theory. In the problem considered, the only remaining phenomena that is open for a more accurate modelling is the impact event itself and therefore a more refined impact model than the one presented here seems worthwhile to pursue.

However, in this presentation, an approach is tested where an impact is interpreted as a process consisting of a series of two, three or even more bounces between the beam and the constraint before the process is regarded as completed. This impact process is also recognized in experiments and the time of duration of this process can be measured and compared to simulations. An excellent agreement between simulations and experimental results has then been obtained.

REFERENCES

1. G. X. Li, M. P. Paidoussis and F. C. Moon 1989 *Journal of Sound and Vibration* **135**, 1–19. Chaotic oscillations of the autonomous system of a constrained pipe conveying fluid.
2. F. C. Moon and S. W. Shaw 1983 *International Journal of Non-Linear Mechanics* **18**, 465–477. Chaotic vibrations of a beam with non-linear boundary conditions.
3. I. Svensson 1993 *Licentiate Thesis LUTFD2/(TFHF-1014)/1-68/(1993), Department of Solid Mechanics, Lund Institute of Technology, Lund, Sweden.* Dynamic Buckling of a Beam with Transverse Constraints.
4. I. Svensson 1996 *Nonlinear Dynamics* **11**, 315–328. Dynamic buckling of a beam with transverse constraints.
5. A. N. Kounadis 1977 *Journal of Applied Mechanics* **44**, 731–736. Stability of elastically restrained Timoshenko cantilevers with attached masses subjected to a follower force.
6. A. N. Kounadis 1979 *Zeitschrift für Angewandte Mathematik und Mechanik* (*ZAAM*), **59**, 523–531. Dynamic snap-through buckling of a Timoshenko two bar frame under a suddenly applied load.
7. Y. C. Fung 1995 *Foundations of Solid Mechanics.* Englewood Cliffs, NJ: Prentice-Hall.
8. J. Lemaitre and J.-L. Chaboche 1990 *Mechanics of Solid Materials.* Cambridge: Cambridge University Press.
9. S. R. Timoshenko, D. H. Young and W. Weaver Jr. 1974 *Vibration Problems in Engineering.* New York: John Wiley.
10. G. R. Cowper 1966 *Journal of Applied Mechanics* **33**, 335–340. The shear coefficient in Timoshenko's beam theory.
11. N. W. Lachlan 1964 *Theory and Application of Mathieu Functions.* New York: Dover Publications.
12. *Matlab Reference Guide.* August 1992.